Experimentally testing impedance boundary conditions for acoustic liners with flow: beyond upstream and downstream[1]

André Mateus Netto Spillere[a,*], Lucas Araujo Bonomo[a], Júlio Apolinário Cordioli[a], Edward James Brambley[b]

[a] *Department of Mechanical Engineering, Federal University of Santa Catarina, 88040-900 Florianópolis, Brazil*
[b] *Mathematics Institute and WMG, University of Warwick, Coventry CV4 7AL, United Kingdom*

Abstract

Impedance eduction experiments on acoustic liners with flow have systematically shown the educed impedance depending on the direction of the incident wave. Recent attempts to model this dependence include impedance boundary conditions with an additional degree of freedom. In this case, both upstream and downstream acoustic sources must be used to educe both the liner impedance and the extra degree of freedom of the model, which implies two different axial wavenumber conditions are used, and always result in a perfect collapse of the educed impedances; this would be true whether or not the model itself is correct. In this work, we describe a novel experimental setup that allows for four different axial wavenumbers per frequency to be measured: two upstream and two downstream. We use this experiment to investigate three different impedance boundary conditions, namely inviscid sheared, viscous, and momentum transfer conditions, in addition to the classical Ingard–Myers boundary condition, using an inverse eduction technique based on the mode matching method. The additional degree of freedom in each of the first three models is best fitted to experimental data, and then compared to the theoretically predicted values. Unphysical or unrealistic values are found at certain frequencies for each model, and therefore the validity of such models is questionable. The predictive capabilities of the models are tested and compared by means of the plane-wave scattering matrix, and no model is found to be truly predictive. Under certain conditions, educed impedances using the Ingard–Myers boundary condition show similar accuracy in terms of transmission coefficients when compared to the other models.

Keywords: acoustic liners, boundary conditions, impedance eduction, mode matching, scattering matrix

1. Introduction

Acoustic liners are used in aircraft engines as noise reducing materials, the simplest construction being a honeycomb layer topped by a perforate face-sheet and backed by a rigid plate. These are commonly represented by their locally reacting acoustic impedance $Z(\omega)$, which can be used as a boundary condition in models or simulations of aircraft engine noise. Experimental techniques may be used to educe this liner impedance under realistic flight conditions. In particular, flow effects are of primary interest since they change the oscillatory behaviour at the face-sheet holes, and consequently the acoustic impedance. In principle, the impedance should remain independent of the incident acoustic field, but recent evidence has shown that a discrepancy is found when the wave propagation direction is changed [2–4]. In other words,

[1] A preliminary version of some parts of this paper was presented as AIAA Paper 2019-2488 at the 25th AIAA/CEAS Aeroacoustics Conference in Delft, The Netherlands [1].

[*] Corresponding author

Email addresses: andre.spillere@lva.ufsc.br (André Mateus Netto Spillere), lucas.bonomo@lva.ufsc.br (Lucas Araujo Bonomo), julio.cordioli@ufsc.br (Júlio Apolinário Cordioli), E.J.Brambley@warwick.ac.uk (Edward James Brambley)

experiments educe different impedances for the same liner when using either upstream- or downstream-propagating sound, indicating flaws in the modelling used to educe the impedances.

Most of the experimental methods rely on a duct propagation model, with uniform flow and the Ingard–Myers [5, 6] boundary condition the most common assumptions. Several attempts have been made to include governing equations and boundary conditions that capture the actual physics. However, Weng et al. [4] concluded that viscosity is not able to account for the discrepancy between upstream and downstream and collapse the educed impedances onto one value per frequency, while Nark et al. [7] found that small corrections to the mean flow velocity were sufficient to collapse the upstream and downstream educed impedances. More recently, Roncen et al. [8] concluded that this inconsistency is still present even when considering a three-dimensional inviscid sheared flow profile and no-slip condition at the lined wall, suggesting the liner physics are still not fully captured. With this is mind, novel boundary conditions have been introduced in the past years by including an additional parameter to better describe the liner physics [9, 10]. In the context of impedance eduction, modelling these additional parameters is usually replaced by best-fitting to experimental data [2, 4]. However, in a conventional impedance eduction experiment, only two different axial wavenumbers k are excited and measured at each frequency, namely the upstream and downstream propagating plane waves. Therefore, any additional parameter will require measurements with both upstream and downstream acoustic sources in order to be educed, necessarily giving a single value for the impedance and another for the free parameter, irrespective of the validity of the model. This leaves the validity of these models as an open question. In particular, it is unclear how predictive the educed impedance and the model will be when used in situations beyond the experimental apparatus the impedance was educed in, such as when exposed to multiple higher-order azimuthal modes in actual aircraft engines, or to different flow profiles.

In this work, we describe an experiment that allows the investigation of four axial wavenumbers per frequency, with the same acoustic lining and the same flow, which can be achieved with indepedent measurements using one and two lined walls. Here, the single lined wall case is used to educe liner impedance and any additional wavenumber-independent parameter, whereas the two lined wall case is used to test the predictive capacity of each model. The educed additional parameters are also compared to their theoretically predicted values, when available. The main objective of this work is to identify physically accurate boundary conditions for acoustic liners in the presence of flow.

This work is organised as follows. Section 2 introduces three different boundary conditions, namely inviscid sheared, viscous, and momentum transfer, besides the classical Ingard–Myers condition. Section 3 describes the experimental setup and Section 4 presents an impedance eduction technique based on the mode-matching method. In Section 5, impedance and additional parameters are educed with one lined wall, and then tested with two lined walls. The main conclusions are presented in Section 6.

2. Boundary conditions

A mean flow over the surface of the acoustic liner modifies the normalised effective impedance $Z_{\text{eff}}(\omega, k)$ seen by an acoustic field within that mean flow, so that

$$Z_{\text{eff}} = \frac{\tilde{p}}{(\tilde{\boldsymbol{v}} \cdot \boldsymbol{n})}, \tag{1}$$

with $\tilde{p}$ the acoustic pressure, $\tilde{\boldsymbol{v}}$ the acoustic velocity and $\boldsymbol{n}$ the normal vector pointing into the wall. The effective impedance $Z_{\text{eff}}(\omega, k)$ is a function of the actual normalised impedance $Z(\omega)$ of the acoustic liner, frequency ω and Mach number M, with the exact dependence depending on the boundary condition assumed.

2.1. Ingard-Myers boundary condition

Traditionally, the Ingard–Myers [5, 6] boundary condition is used to model the effects of non-uniform mean flow on the acoustic propagation in the immediate neighbourhood of the lined surface, and results in

$$Z_{\text{eff}} = \frac{\omega Z}{\omega - Mk}, \tag{2}$$

where M is the slipping velocity of the mean flow at the liner surface which, in the context of this work, also denotes the bulk Mach number. The Ingard–Myers boundary condition enforces continuity of acoustic displacement across an infinitely thin inviscid boundary layer to the leading order [11]. Even if the liner is locally reacting, so that $Z(\omega)$ is independent of the wavenumber k, the Ingard–Myers boundary condition shows that the effective impedance $Z_{\text{eff}}(\omega, k)$ is no longer locally reacting, but depends on the wavenumber k. In theory, it should still be possible to recover the impedance $Z(\omega)$ from the effective impedance $Z_{\text{eff}}(\omega, k)$, with measurements from a downstream or upstream source producing the same results. However, experimental tests carried out on different test configurations and using different impedance eduction techniques have consistently shown different results from upstream and downstream sources [2–4, 7]. Since the only difference between upstream- and downstream-propagating plane waves is their axial wavenumber k, this is evidence that the k-dependence of the impedance boundary model $Z_{\text{eff}}(\omega, k)$ being used to educe the impedance is incorrect.

It is important to emphasise that Ingard–Myers boundary condition, as well as the other boundary conditions considered in this work, do not intend to model the effect of the mean flow on the liner impedance itself, as done by other models in the literature [12, 13]. These impedance models aim to account for the effects of geometry, temperature, mean flow and sound pressure level on the actual impedance response of the liner itself, while the boundary conditions are used to model the effect of a sheared mean flow on the acoustic field in the vicinity of a treated surface with a given impedance. While clearly related, these are different effects.

2.2. Brambley boundary condition

Recently, it was shown that the Ingard–Myers boundary condition is illposed and leads to unphysical instability in models and simulations [14]. The illposed behaviour is removed by accounting for a thin inviscid mean flow boundary layer within the impedance boundary condition, leading to a significantly more complicated dependence of Z_{eff} on the axial wavenumber k. Such dependence is represented as

$$Z_{\text{eff}} = \frac{\mathrm{i}\omega Z + (\omega - Mk)^2 \delta I_0}{\mathrm{i}(\omega - Mk) - \omega Z k^2 \delta I_1/(\omega - Mk)}, \tag{3}$$

with

$$\delta I_0 = \int_0^\delta 1 - \frac{(\omega - U(y)k)^2 \rho(y)}{(\omega - Mk)^2} \,\mathrm{d}y\,, \tag{4a}$$

$$\delta I_1 = \int_0^\delta 1 - \frac{(\omega - Mk)^2}{(\omega - U(y)k)^2 \rho(y)} \,\mathrm{d}y\,, \tag{4b}$$

where $U(y)$ and $\rho(y)$ are the mean flow velocity and density within the boundary layer, δ is the thickness of the boundary layer, and outside the boundary layer $U = M$ and $\rho = 1$. Application of this boundary model in the eduction process was found to reduce but not eliminate the discrepancy between upstream- and downstream-educed impedances [15]. In this work, a different approach is considered by taking as a free parameter the thickness δ of a linear boundary layer profile with uniform density, leading to a simplified model in the form

$$Z_{\text{eff}} = \frac{\mathrm{i}\omega Z - \omega k M \delta + \frac{2}{3} k^2 M^2 \delta}{\mathrm{i}(\omega - Mk) - Z k^3 M \delta/(\omega - Mk)}. \tag{5}$$

In theory, the educed δ should be a constant independent of frequency.

It should be emphasised that this, and subsequent, boundary conditions account for a boundary layer over the lined surfaces only. Boundary layers over rigid surfaces result in a much smaller modifications of the rigid-walled boundary condition of an order neglected in this and most other studies. This justifies our use of this boundary condition only in the y direction in what follows, despite the three-dimensional nature of the experiment.

2.3. Viscous boundary condition

Further boundary conditions attempt to model the effects of viscosity within the thin boundary layer at the impedance wall [10, 16–18], of which the most notable for its simplicity is that of Aurégan et al. [10]. Neglecting thermal effects (as per Renou and Aurégan [2]), this boundary condition in the present notation is given by

$$Z_{\text{eff}} = \frac{\omega Z}{\omega - (1-\beta)Mk}, \tag{6}$$

with

$$\beta = \frac{1}{M}\int_0^\delta \frac{\mathrm{d}U}{\mathrm{d}y} \exp\left(-y\sqrt{\mathrm{i}\omega/\nu}\right) \mathrm{d}y\,, \tag{7}$$

where ν is the kinematic viscosity. The factor βM can be interpreted as an effective Mach number related to the added displacement due to shear stress at the lined wall [10]. Renou and Aurégan [2] showed that if the formula for β in (7) is ignored and instead β is best-fitted to experimental results, then the upstream and downstream educed impedances can be made to collapse onto a single curve, and moreover that the inferred β performs as expected, with $\beta \approx 0$ at high frequencies (continuity of normal acoustic displacement) and $\beta \approx 1$ at low frequencies (continuity of acoustic velocity).

2.4. Momentum transfer boundary conditions

Another class of boundary conditions has been recently proposed, and it includes an extra parameter representing the transfer of axial momentum between the fluid and the liner, characterized by the acoustic shear stress at the liner surface, $\tilde{\tau}_w$. Schulz et al. [19] model the axial momentum transfer as depending on the normal velocity, using a momentum transfer impedance $\zeta = \tilde{\tau}_w/(\tilde{\boldsymbol{v}} \cdot \boldsymbol{n})$. In contrast, Aurégan [20] models the axial momentum transfer as depending on the pressure, using a friction factor $f_w = \tilde{\tau}_w/\tilde{p}$. While Schulz et al. [19] apply their stress boundary condition within a linearised Navier-Stokes equation solver instead of the no slip condition, Aurégan [20] derives an effective impedance Z_{eff} under suitable simplifying assumptions, resulting in

$$Z_{\text{eff}} = \frac{\omega Z}{(\omega - Mk)(1 + k\zeta/\omega)} = \frac{\omega Z}{(\omega - Mk)(1 + kf_w Z/\omega)}. \tag{8}$$

Although the momentum transfer boundary condition resembles Eq. (6), it should be noted that they have a different dependence on k.

3. Experimental setup

3.1. Test rig description

We consider the situation shown schematically in Fig. 1, with a rectangular duct containing a steady mean flow of velocity $U(y)$ in the positive z direction. The duct contains a liner test section, where both the upper and lower surfaces can be either lined or unlined (rigid-walled) with an acoustic impedance Z. Upstream and downstream of the test section are 1/4-inch flush-mounted Brüel and Kjær 4944-A microphones, and beyond these are two or more wall-mounted Beyma CP855-Nd compression drivers. Quasi-anechoic terminations are placed at both duct exits, ensuring a reflection coefficient below 0.2 for all frequencies of interest at no-flow condition. For any given setup of the test section, measurements are made by all microphones for harmonic excitation using either an upstream or downstream loudspeaker.

The duct cross-section is given by a height of $2H = 4\,\text{cm}$, and width $2W = 10\,\text{cm}$, for which the no-flow cut-on frequency for the first transverse mode is 1700 Hz. Since the microphones are positioned at half of the duct height, they are on the nodal line for this first higher order mode, and hence this mode is not captured [21], which is confirmed by comparing the educed impedance without flow to results obtained with a normal incidence impedance tube. The second transverse mode cuts on at 3400 Hz, and so the frequency range tested is from 500 Hz to 2500 Hz in this study. The lined section accommodates liners of length up to 210 mm, although in this study the effective liner length is 171 mm.

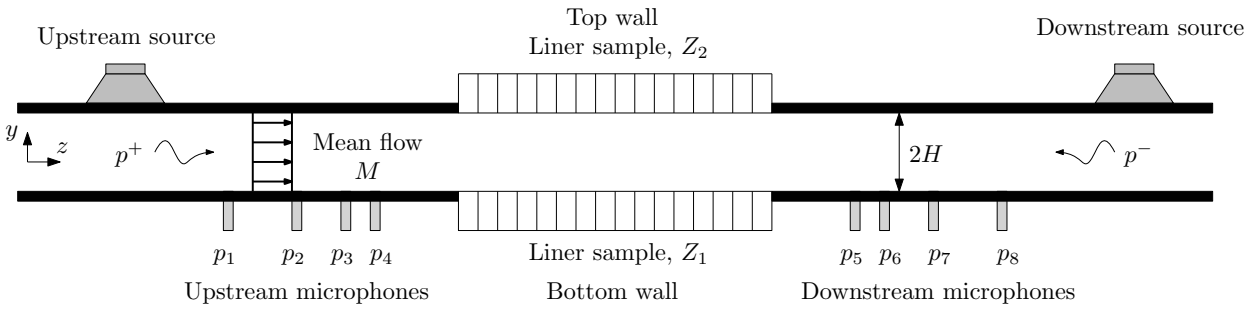

Figure 1: Schematic top view of the experiment.

Two identical liners were supplied by UTC Aerospace Systems (now Collins Aerospace), being conventional one-degree-of-freedom honeycomb liners. The liner cavities were 48.6 mm deep, with 1 mm thick facing sheets, 1 mm diameter holes and a 7.4 % open area. These parameters were verified experimentally using a normal incidence impedance tube; the liners were found to be identical, apart from a slight variation of approximately 0.1 % in the effective percentage of open area.

3.2. Data processing

The data from the microphones are post-processed to infer the transmitted and reflected acoustic waves, from which the impedance of the liner used in the test section may be educed, as detailed in Section 4. The loudspeakers produce an incident wave with a sound pressure level of 130 dB, which maximise signal-to-noise ratio without triggering non-linear effects. The pressure measurements are processed into complex frequency response functions $p_q^{\text{exp}}(\omega)$ at each microphone $q = 1, \ldots, 8$, using Welch's method [22, p. 342–345] and the H_1 estimator [22, p. 350–351] with the loudspeaker input signal as a noise-free reference. Data were sampled at 12.8 kHz and for each frequency, 30 averages of 12 800 samples each with 75 % of overlap were considered. At frequencies of high attenuation, such as in the two lined walls case, the number of averages was increased up to 420. Microphones were calibrated in amplitude and phase relative to each other by exposing them to the same acoustic field [23].

The flow is driven by a compressed air reservoir, with a control system regulating the valve opening to maintain a constant Mach number. A 2 mm diameter Pitot tube with a KIMO CP-113 pressure transmitter and a KIMO TM-110 temperature transmitter are located at the upstream section to measure the centreline Mach number, which is used as a target value by the control system. Results are presented for bulk Mach numbers of approximately 0.2 and 0.3, calculated by averaging over the duct cross-section using a quadrature method [24].

3.3. Flow profile

As described in Section 2, the boundary conditions may depend on the velocity profile of the mean flow. In order to measure the velocity profile in the test rig, the liner section was replaced by a rigid wall section of same length containing a small aperture to allow the introduction of a Pitot tube and a static pressure tap. The Pitot tube was placed at half of the duct height and half length of the test section. Measurements were taken in steps of approximately 1 mm in the span-wise direction for two different mean flow velocities.

In order to estimate the velocity gradients, we consider the following fully developed turbulent flow profile [25, p. 566–571]

$$\frac{U}{U_\tau} = y^+, \qquad y^+ \leq 15, \tag{9a}$$

$$\frac{U_m - U}{U_\tau} = 5.75 \log_{10}\left(\frac{H}{\eta}\right), \qquad y^+ > 15, \tag{9b}$$

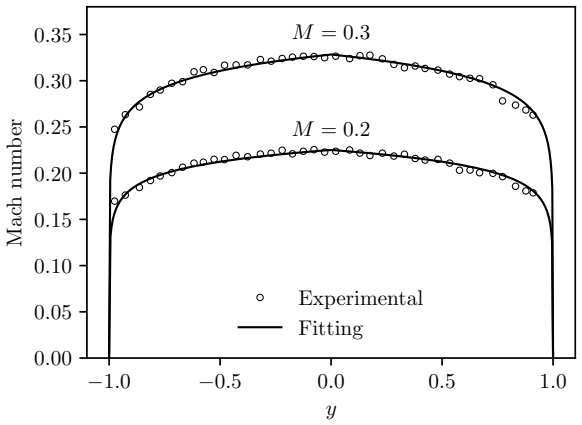

Figure 2: Measured velocity profile at the duct centreline and least-squares fitting to Eq. (9).

valid for $0 < \eta < H$, where $y^+ \equiv \eta U_\tau/\nu$ is the distance from the wall in viscous lengths, $U_\tau \equiv \sqrt{\tau_\mathrm{w}/\rho_0}$ is the friction velocity, U_m is the maximum velocity and $\log_{10}$ is the decimal logarithm. Notice that we use an auxiliary coordinate $\eta \equiv H(y+1)$ due to our choice of coordinate system for the acoustic field, as described in the next section. Moreover, we assume that viscous contributions dominate the flow profile up to $y^+ \approx 15$, and turbulent processes dominate in the remaining portion of the duct. The measurements were fitted using a least-squares algorithm, and the results are shown in Fig. 2. For each bulk velocity $M = 0.2$ and $M = 0.3$, the friction velocities are found to be, respectively, $U_\tau = 2.54\,\mathrm{m\,s^{-1}}$ and $U_\tau = 3.53\,\mathrm{m\,s^{-1}}$.

Of special interest, we seek an equivalent boundary layer thickness of a linear profile to be compared with the δ introduced in Section 2.2. It is known that velocity profiles with the same boundary layer displacement thickness provide similar levels of acoustic attenuation [26]. For this particular turbulent flow profile, the boundary layer displacement thickness δ^* can be estimated by

$$\delta^* = \int_0^H \left(1 - \frac{U}{U_m}\right) \mathrm{d}\eta \;\approx\; \delta_v \;-\; \frac{U_\tau^2 \delta_v^2}{2 U_m \nu} \;+\; 2.5 \frac{U_\tau}{U_m}\left(H - \delta_v\left(\ln\left(\frac{H}{\delta_v}\right) + 1\right)\right), \tag{10}$$

where $\delta_v \equiv 15\nu/U_\tau$ is the viscous sublayer thickness. In a linear boundary layer profile, it can be shown [27] that $\delta^*/\delta = 0.5$, and therefore an effective thickness of $\delta = 2\delta^*$ should be expected in the test rig. Due to the three-dimensional nature of duct flows, this value should be taken as a reference estimate.

4. Impedance eduction

In order to educe the liner impedance, a numerical solution of the acoustic field is necessary. In this case, we choose the mode-matching method due to its accuracy and reduced computational cost, which are crucial characteristics for inverse techniques. We consider a different approach from Elnady et al. [28] and Aurégan et al. [29] by solving the governing equations with a pseudospectral method, together with an improved matching condition.

It has been shown in the literature [30] that inverse techniques display similar results to other eduction methods, including the so-called direct methods based on Prony-like algorithms [31], which also present a wave-direction dependence of the educed impedance [2, 4]. However, the required microphone arrangement does not support two lined walls, and therefore it has not been considered for this study.

4.1. Generalised eigenvalue problem

Although closed-form results are known for wavenumbers in a lined section with uniform flow [28], it is necessary to solve the eigenvalue equation with a tracking method [32]. This procedure may be too costly

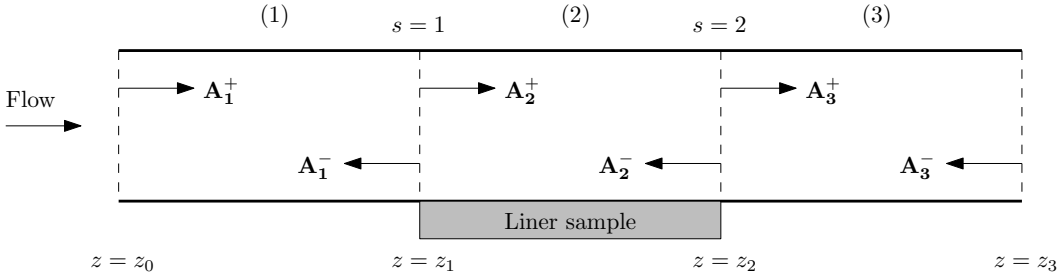

Figure 3: Downstream and upstream modal amplitudes, respectively $\mathbf{A_i^+}$ and $\mathbf{A_i^-}$, at each duct section.

when several modes are required and complicated when surface waves are present. An alternative approach is to use Chebyshev polynomials as basis functions and solve the boundary value problem at each collocation point, leading to a linear eigenvalue problem. A similar procedure has been adopted by Aurégan et al. [29], although there a Galerkin method with rigid-walled acoustic modes as basis functions was used.

Consider a straight bi-dimensional rectangular duct with uniform flow in z direction, constant speed of sound c_0 and density ρ_0. Assuming acoustic modes of the form $\tilde{p}(y)\mathrm{e}^{\mathrm{i}\omega t - \mathrm{i}kz}$, acoustic pressure perturbation is governed by the convected Helmholtz equation, given by

$$\frac{\mathrm{d}^2\tilde{p}}{\mathrm{d}y^2} + \Big((\omega - Mk)^2 - k^2\Big)\tilde{p} = 0, \tag{11a}$$

$$\mathrm{i}(\omega - Mk)\tilde{u} - \mathrm{i}k\tilde{p} = 0, \tag{11b}$$

$$\mathrm{i}(\omega - Mk)\tilde{v} + \frac{\mathrm{d}\tilde{p}}{\mathrm{d}y} = 0, \tag{11c}$$

where $\tilde{u}$ and $\tilde{v}$ are respectively the axial and transverse acoustic velocities. Eq. (11a) can be solved by means of a pseudospectral algorithm, which is essentially a N-th order finite difference method [33, p. 98]. By introducing an auxiliary variable $\tilde{q} = k\tilde{p}$, the axial wavenumbers and respective mode shapes are given by the generalised eigenvalue problem

$$\begin{bmatrix} \mathbf{D}^2 + \omega^2\mathbf{I} & \mathbf{0} \\ \mathbf{0} & \mathbf{I} \end{bmatrix} \begin{bmatrix} \mathbf{p} \\ \mathbf{q} \end{bmatrix} = k \begin{bmatrix} 2\omega M\mathbf{I} & \left(1 - M^2\right)\mathbf{I} \\ \mathbf{I} & \mathbf{0} \end{bmatrix} \begin{bmatrix} \mathbf{p} \\ \mathbf{q} \end{bmatrix}, \tag{12}$$

with $\mathbf{p}$ and $\mathbf{q}$ vectors containing p_i and q_i at each collocation point $i = 0, ..., N$, $\mathbf{I}$ the identity matrix, $\mathbf{0}$ the zero matrix and $\mathbf{D}$ the differentiation matrix for a Gauss–Lobatto grid of $N+1$ points [33, p. 570]. Boundary conditions are applied at rows corresponding to $i = 0$ and $i = N$ by combining Eq. (11c) with the effective impedance. The eigenvalue problem is solved with a QZ algorithm [33, p. 129] and $N = 100$, which gives excellent accuracy for the purposes of this work. Possible unstable surface waves are excluded [14], upstream modes are given by $\mathrm{Im}(k_n^{\pm}) > 0$ and downstream modes by $\mathrm{Im}(k_n^{\pm}) < 0$. The acoustic modes are ordered in ascending values of $\mathrm{Re}(\alpha_n)$, where α is the transverse wavenumber, related to the axial wavenumber by

$$\left(\alpha_n^{\pm}\right)^2 = \left(\omega - Mk_n^{\pm}\right)^2 - \left(k_n^{\pm}\right)^2. \tag{13}$$

In the rigid-walled sections, it is possible to show that the transverse wavenumbers are given by $\alpha_n^{\pm} = (n-1)\pi/2$, $n = 1, ..., \mathcal{N}$. Therefore, the acoustic field can be approximated at each section $j = 1, 2, 3$ as a sum of $\mathcal{N}$ acoustic modes (see Fig. 3), so that

$$p^{(j)}(y, z) = \sum_{n=1}^{\mathcal{N}} \Big(A_n^{(j)+}\psi_n^{(j)+}(y)\mathrm{e}^{-\mathrm{i}k_n^{(j)+}z} + A_n^{(j)-}\psi_n^{(j)-}(y)\mathrm{e}^{-\mathrm{i}k_n^{(j)-}z}\Big), \tag{14}$$

where $A_n^{\pm}$ are the modal amplitudes. Note that we do not assume perfectly anechoic terminations, so that in general $A_1^{(1)+}$ and $A_1^{(3)-}$ are nonzero and will be determined during the eduction process. This is to

avoid anomalies resulting from incorrectly specifying upstream or downstream boundary conditions, such as assuming anechoic terminations [34].

4.2. Matching condition

The most commonly used procedure to match the acoustic field at each interface is to consider continuity of pressure and velocity [28, 35, 36]. However, a more general approach is to consider continuity of mass and momentum across the interface as proposed by Gabard and Astley [37] which, in the present notation, reads

$$(1-M^2)\int_S \overline{f}\left(p^{(s+1)}-p^{(s)}\right)\mathrm{d}S - M^2\oint_\Gamma \overline{f}\left(\boldsymbol{\xi}^{(s+1)}-\boldsymbol{\xi}^{(s)}\right)\cdot\boldsymbol{n}\,\mathrm{d}\Gamma = 0, \tag{15a}$$

$$(1-M^2)\int_S \overline{f}\left(u^{(s+1)}-u^{(s)}\right)\mathrm{d}S + M\oint_\Gamma \overline{f}\left(\boldsymbol{\xi}^{(s+1)}-\boldsymbol{\xi}^{(s)}\right)\cdot\boldsymbol{n}\,\mathrm{d}\Gamma = 0, \tag{15b}$$

where $s = 1, 2$ denotes the interface number, S is the duct cross-section, Γ is the interface contour, $\overline{f}$ is a suitable complex conjugate test function, and $\boldsymbol{\xi}$ is the acoustic displacement,

$$\tilde{\boldsymbol{\xi}}\cdot\boldsymbol{n} = \frac{\tilde{p}}{\mathrm{i}(\omega - Mk)Z_{\mathrm{eff}}}. \tag{16}$$

Although the edge contribution may be minimal in the context of impedance eduction, it plays an important role in the plane-wave scattering matrix prediction [38]. Note that the boundary integral depends on the assumed boundary condition through $\boldsymbol{\xi}$, and consequently Z_{eff}.

Substituting Eq. (14) into (15a) and (15b) leads to the following system of equations

$$\begin{bmatrix}\mathbf{P_2^+} & -\mathbf{P_1^-}\\ \mathbf{M_2^+} & -\mathbf{M_1^-}\end{bmatrix}\begin{bmatrix}\mathbf{A_2^+}\\ \mathbf{A_1^-}\end{bmatrix} = \begin{bmatrix}\mathbf{P_1^+} & -\mathbf{P_2^-}\\ \mathbf{M_1^+} & -\mathbf{M_2^-}\end{bmatrix}\begin{bmatrix}\mathbf{E_1^+}(z_1-z_0) & \mathbf{0}\\ \mathbf{0} & \mathbf{E_2^-}(z_1-z_2)\end{bmatrix}\begin{bmatrix}\mathbf{A_1^+}\\ \mathbf{A_2^-}\end{bmatrix}, \tag{17a}$$

$$\begin{bmatrix}\mathbf{P_3^+} & -\mathbf{P_2^-}\\ \mathbf{M_3^+} & -\mathbf{M_2^-}\end{bmatrix}\begin{bmatrix}\mathbf{A_3^+}\\ \mathbf{A_2^-}\end{bmatrix} = \begin{bmatrix}\mathbf{P_2^+} & -\mathbf{P_3^-}\\ \mathbf{M_2^+} & -\mathbf{M_3^-}\end{bmatrix}\begin{bmatrix}\mathbf{E_2^+}(z_2-z_1) & \mathbf{0}\\ \mathbf{0} & \mathbf{E_3^-}(z_2-z_3)\end{bmatrix}\begin{bmatrix}\mathbf{A_2^+}\\ \mathbf{A_3^-}\end{bmatrix}, \tag{17b}$$

where $\mathbf{P}$ and $\mathbf{M}$ are projection matrices, $\mathbf{E}$ are propagation matrices, details of which are shown in Appendix A, and $\mathbf{A}$ are modal amplitude vectors. For a given $\mathbf{A_1^+}$ and $\mathbf{A_3^-}$, Eqs. (17a) and (17b) can be solved with a simple iterative routine [39]. The modal amplitudes at rigid-walled sections are also related by the scattering matrix,

$$\begin{bmatrix}\mathbf{A_3^+}\\ \mathbf{A_1^-}\end{bmatrix} = \begin{bmatrix}\mathbf{T^+} & \mathbf{R^-}\\ \mathbf{R^+} & \mathbf{T^-}\end{bmatrix}\begin{bmatrix}\mathbf{A_1^+}\\ \mathbf{A_3^-}\end{bmatrix}, \tag{18}$$

which can be experimentally determined using a two-source technique [40]. In other words, measurements with independent upstream and downstream acoustic sources are necessary to compute the scattering matrix, which is already performed to educe the additional parameters. Of special interest is the plane-wave scattering matrix, given by

$$\begin{bmatrix}A_1^{(3)+}\\ A_1^{(1)-}\end{bmatrix} = \begin{bmatrix}T^+ & R^-\\ R^+ & T^-\end{bmatrix}\begin{bmatrix}A_1^{(1)+}\\ A_1^{(3)-}\end{bmatrix}. \tag{19}$$

4.3. Eduction procedure

The impedance eduction procedure is described as follows. At each frequency, the measured acoustic pressure at rigid-walled sections is decomposed into upstream and downstream propagating plane waves. Viscothermal losses are accounted for by corrections in the plane-wave axial wavenumber [41], such that

$$k_1^{\pm} = \frac{\pm\omega K_0}{(1 \pm K_0 M)}, \tag{20}$$

with K_0 being the first order Kirchhoff solution given by

$$K_0 = 1 + \frac{1-\mathrm{i}}{\mathrm{Sh}\sqrt{2}}\left(1 + \frac{\gamma-1}{\sqrt{\mathrm{Pr}}}\right), \tag{21}$$

where $\mathrm{Sh} = r_h\sqrt{\omega/\nu}$ is the shear wavenumber, r_h is the hydraulic radius, $\gamma \approx 1.4$ is the heat capacity ratio and $\mathrm{Pr} \approx 0.7$ is the Prandtl number. Using all four microphones at each section leads to an over-determined system. For test section 1, it is given by

$$\begin{bmatrix} \exp\left(-\mathrm{i}k_1^+ z_1\right) & \exp\left(-\mathrm{i}k_1^- z_1\right) \\ \exp\left(-\mathrm{i}k_1^+ z_2\right) & \exp\left(-\mathrm{i}k_1^- z_2\right) \\ \exp\left(-\mathrm{i}k_1^+ z_3\right) & \exp\left(-\mathrm{i}k_1^- z_3\right) \\ \exp\left(-\mathrm{i}k_1^+ z_4\right) & \exp\left(-\mathrm{i}k_1^- z_4\right) \end{bmatrix} \begin{bmatrix} A_1^+ \\ A_1^- \end{bmatrix} = \begin{bmatrix} p_1 \\ p_2 \\ p_3 \\ p_4 \end{bmatrix}, \tag{22}$$

and similarly for test section 3. Solving this system of equations in a least-squares sense for each set of microphones gives the plane wave amplitudes $A_1^{(1)+}$ and $A_1^{(3)-}$, which are used as inputs for the mode matching model. A suitable impedance guess is chosen for the lined wall, for instance by using semi-empirical models based on the liner geometry and flow velocity [12, 13]. Eqs. (17a) and (17b) are then solved assuming $\mathcal{N} = 10$ acoustic modes, which allows the computation of the acoustic field p_q^{num} using Eq. (14) at the location of each microphone q. The cost function $\mathcal{F}$ compares the numerical result to the measurements p_q^{exp} by

$$\mathcal{F}(Z_{\mathrm{eff}}) = \sum_{q=1}^{8} \left| \frac{p_q^{\mathrm{exp}} - p_q^{\mathrm{num}}(Z_{\mathrm{eff}})}{p_q^{\mathrm{exp}}} \right|. \tag{23}$$

The normalization by p_q^{exp} increases the contribution of attenuated waves to the cost function. In practice, it means that the numerical transmission coefficients $|T|$ are being best-fitted to the experimental results.

The cost function is minimised using the Levenberg–Marquardt algorithm [42, 43] until convergence is achieved, which gives the liner impedance. This procedure is performed independently for upstream and downstream acoustic sources when considering Ingard–Myers boundary condition. For the remaining impedance boundary conditions, measurements with upstream and downstream acoustic sources are both considered in the cost function so that

$$\mathcal{F}(Z_{\mathrm{eff}}) = \sum_{q=1}^{8} \left| \frac{p_q^{\mathrm{exp,up}} - p_q^{\mathrm{num,up}}(Z_{\mathrm{eff}})}{p_q^{\mathrm{exp,up}}} \right| + \sum_{q=1}^{8} \left| \frac{p_q^{\mathrm{exp,down}} - p_q^{\mathrm{num,down}}(Z_{\mathrm{eff}})}{p_q^{\mathrm{exp,down}}} \right|. \tag{24}$$

This equation could also be used in conjunction with Ingard–Myers boundary condition, resulting in a single impedance curve. However, it becomes an overdetermined system since two test configurations are used to educe a single parameter, and therefore it has not been applied in this work. The validation of this procedure is presented in Appendix B, together with a discussion of the influence of the matching conditions for impedance eduction and the scattering matrix.

5. Results

5.1. Wave-direction dependence of the educed impedance

Initially, results from using one liner on the bottom of the duct and a rigid wall on the top were compared with using the second liner on the top of the duct and a rigid wall on the bottom. Since the two liners are nominally identical, this comparison highlights any asymmetries in the liners, the liner holders, or the mean flow.

Fig. 4 compares the educed impedance for these two cases. In general, excellent agreement is seen, which confirms the absence of asymmetries in the test rig, test samples and mean flow. Without flow, both samples should exhibit the exact same impedance for both upstream and downstream acoustic sources. The

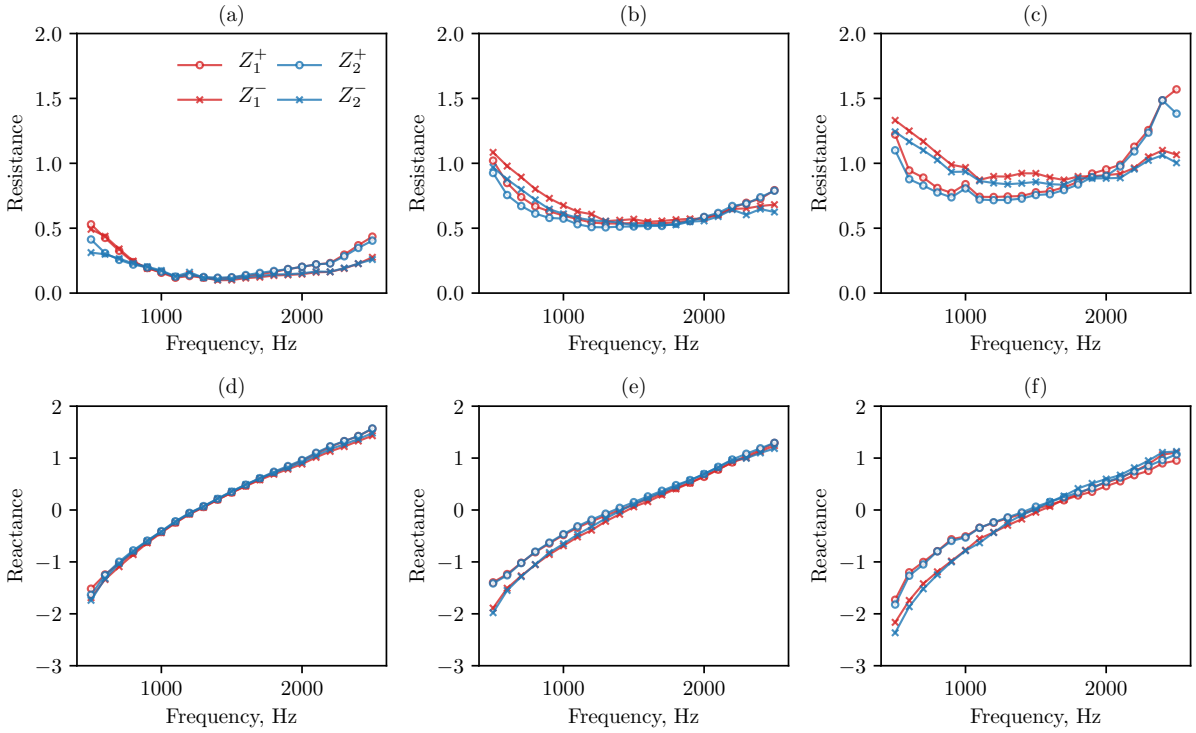

Figure 4: Educed impedance as a function of frequency, for both upstream (+) and downstream (−) acoustic sources, for the lined/rigid (Z_1) and rigid/lined (Z_2) configurations. (a,d) no flow, (b,e) $M = 0.2$, (c,f) $M = 0.3$.

small discrepancy observed at the lower and higher frequency limits are within the uncertainty levels of the test rig, as discussed in Appendix C. In the presence of flow, it is possible to observe the difference between educed impedances using upstream and downstream acoustic sources. Such difference is beyond the uncertainty levels of test rig, even at $M = 0.2$, as also demonstrated in Appendix C. This apparent wave-direction dependence has been systematically reported in the literature [2–4, 7], and contradicts the assumption of a locally reacting wall impedance.

Following Renou and Aurégan [2], another way to verify the educed impedances and their predictive capacity is by means of the plane-wave scattering matrix. Fig. 5 shows the experimental and predicted coefficients of the scattering matrix for the lined/rigid configuration. Predicted coefficients using the upstream educed impedance, and the downstream educed impedance, are both plotted. In the absence of flow, excellent agreement is found with both educed impedances. On the other hand, in the presence of flow, none of the educed impedances is able to correctly predict both upstream and downstream coefficients, again demonstrating the inadequacy of the Ingard–Myers boundary condition. Interestingly, none of the educed impedances are able to correctly predict R^+, which may suggest that the duct propagation model, although numerically validated, is not physically accurate. Similar results were also observed by Yang et al. [38].

5.2. Educing additional parameters

Since using the Ingard–Myers boundary condition gives wavenumber dependent educed impedances, we shall now investigate the two-parameters impedance boundary conditions. In this case, measurements in both upstream and downstream source configurations are used, leading to a single impedance curve, as shown in Fig. 6. Although they are each based on different physical reasoning, all models lead to very similar impedances, which lie, in general, between the upstream and downstream impedances educed using the Ingard–Myers boundary condition.

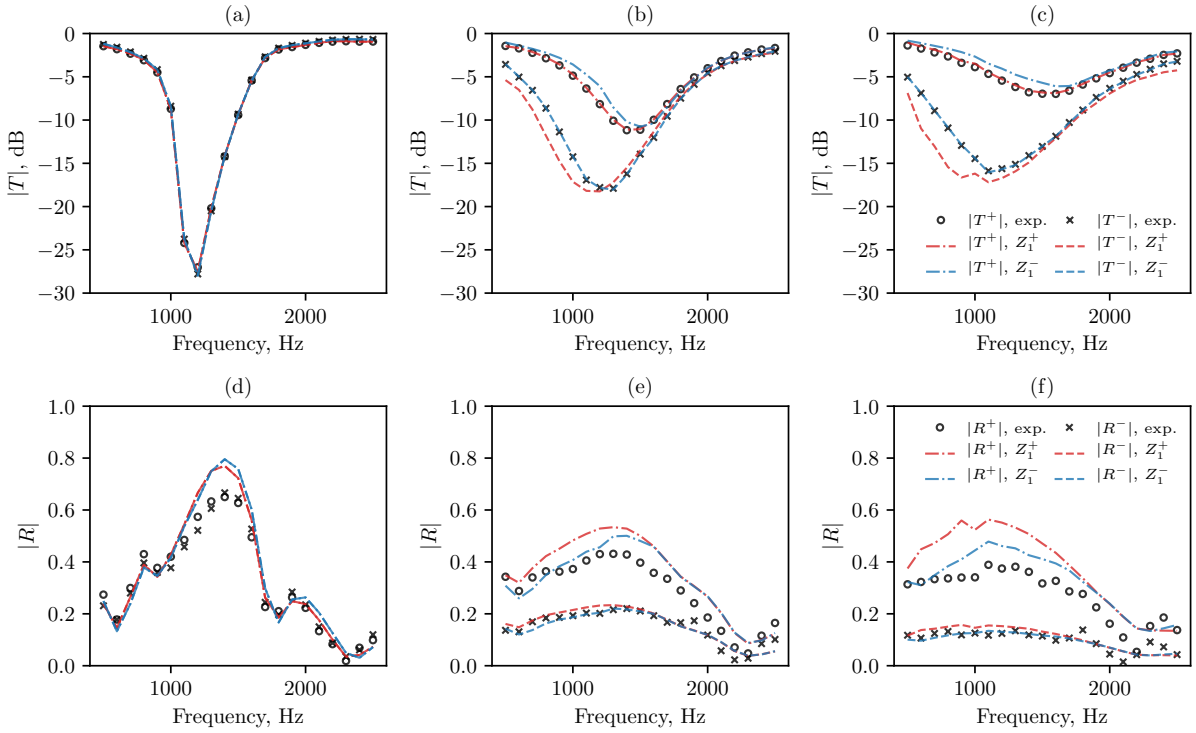

Figure 5: Experimental scattering coefficients for the lined/rigid configuration, and the predicted scattering coefficients using the upstream and downstream educed impedances considering Ingard–Myers boundary condition (Z_1^+ and Z_1^-, respectively). (a,d) no flow, (b,e) $M = 0.2$, (c,f) $M = 0.3$.

Fig. 7 shows the educed boundary layer thickness for both lined/rigid and rigid/lined configuration. In theory, the boundary layer thickness should be unaffected by the presence of liners, and therefore it should remain constant with frequency. The fact that it oscillates, and even becomes negative at certain frequencies, indicates that the fitting is probably unphysical. A negative boundary layer thickness could be related to a strong response of the acoustic field at the liner holes close to the resonance frequency, which can even modify the boundary layer profile [44].

The frequency-dependent educed factor β is shown in Fig. 8, together with the predicted values from Eq. (6). The prediction considers only the velocity profile at the duct centreline, as shown in Fig. 2, whereas the educed β can be seen as a bulk value, and therefore the comparison is more qualitative than quantitative. At Mach number 0.2, the agreement is reasonable up to the resonance frequency. From then on, the real part of the educed β decreases and even becomes negative, which is not predicted by the model. Also, the imaginary part of the educed β, which should remain close to zero [2], starts to increase considerably. This behaviour is more dramatic at Mach number 0.3, which could be related to the low-Mach number limit of the boundary condition. This limitation is inconvenient from the point of view of application to turbofan engines since even higher Mach numbers are expected at take-off condition.

Finally, the educed momentum transfer impedance ζ is shown in Fig. 9. The resemblance to β is striking. In fact, for low Mach numbers and Helmholtz numbers, it is possible to show that $\zeta \approx \beta M$ by comparing Eqs. (6) and (8), which is confirmed in Fig. 9. In the context of impedance eduction in test rigs, it is difficult to show any difference between these two models. In practical terms, unless the prediction in a lined/lined configuration indicates substantially different scattering coefficients, these boundary conditions may be interpreted as equivalent models.

It can be seen in Fig. 10 that the two-parameters models are able to correctly fit both T^+ and T^-. In fact, even the Brambley boundary condition, which accounts for a real-valued additional parameter, can increase

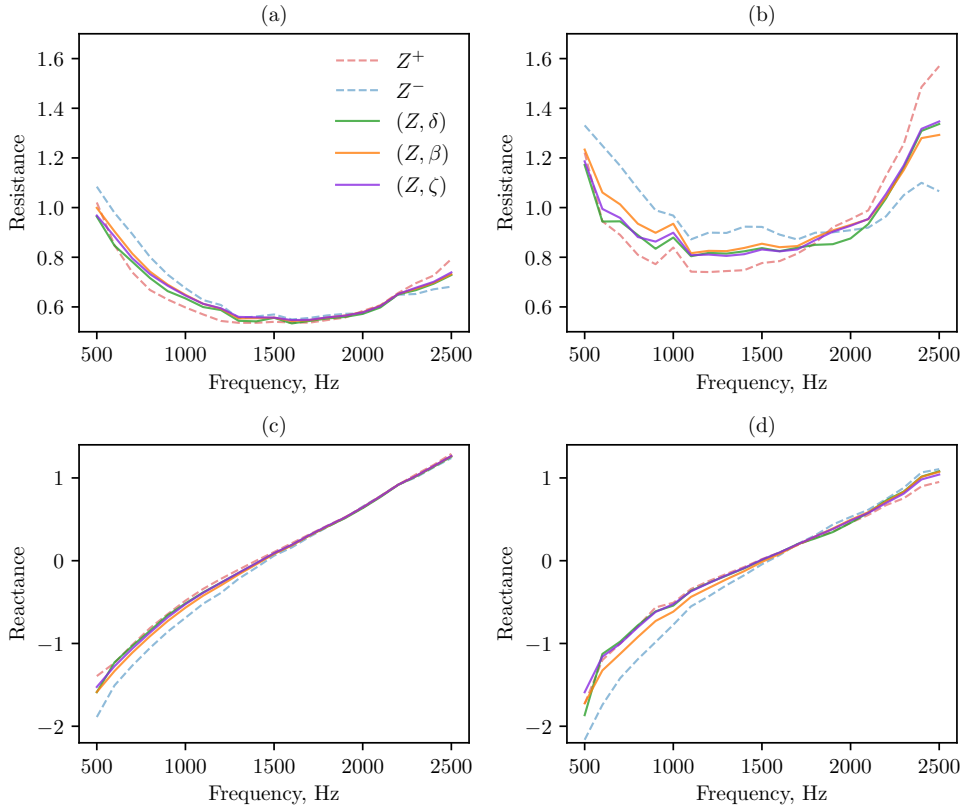

Figure 6: Educed impedances in a lined/rigid configuration using two-parameters models. (a,c) $M = 0.2$, (b,d) $M = 0.3$.

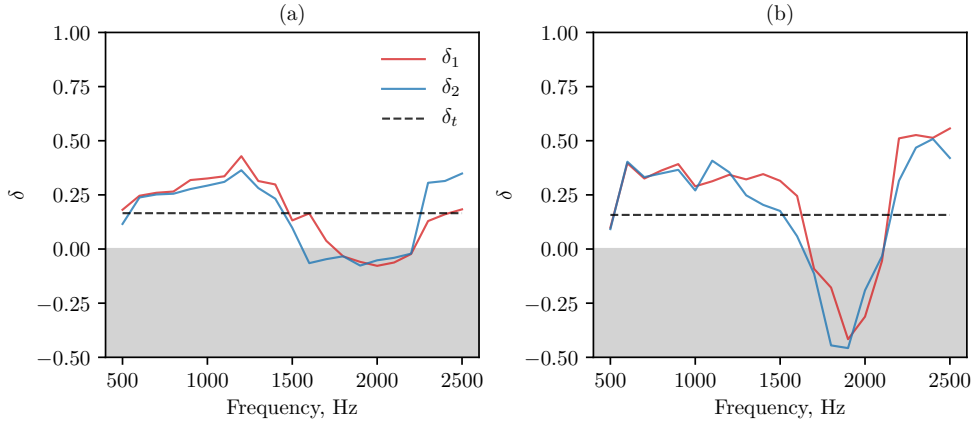

Figure 7: Educed boundary layer thickness for lined/rigid (δ_1) and rigid/lined (δ_2) configurations. Also shown is the theoretical prediction δ_t. (a) $M = 0.2$, (b) $M = 0.3$.

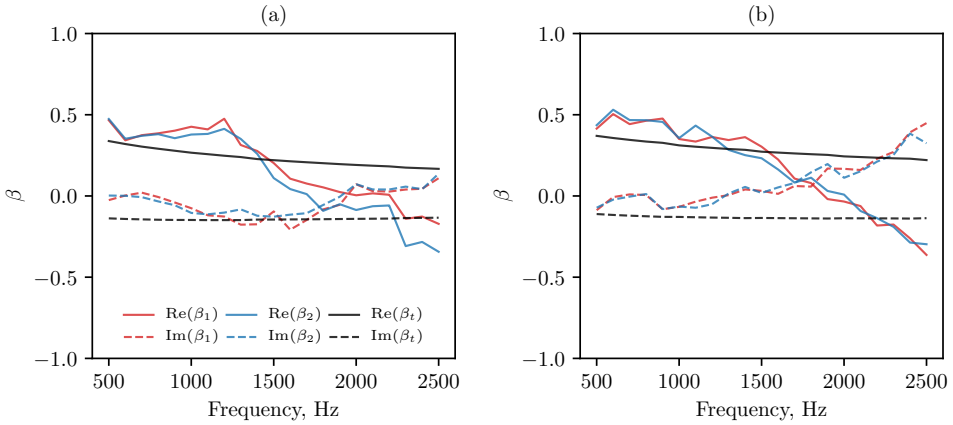

Figure 8: Educed β for lined/rigid (β_1) and rigid/lined (β_2) configurations. Also shown in the theoretical prediction β_t from Eq. (6). (a) $M = 0.2$, (b) $M = 0.3$.

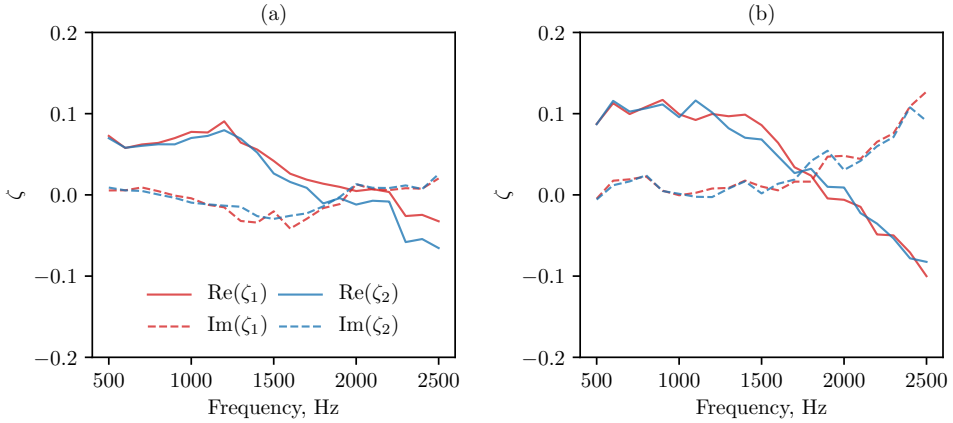

Figure 9: Educed momentum transfer impedance for lined/rigid (ζ_1) and rigid/lined (ζ_2) configurations. (a) $M = 0.2$, (b) $M = 0.3$.

satisfactorily the agreement with the scattering coefficients, when compared to the complex-valued β and ζ. It is interesting to note that none of these models is able to correctly predict R^+, which reinforces the idea that the duct propagation model is still incorrect. We shall next test the impedance models predictive capability by considering a different wavenumber configuration.

5.3. Testing the impedance boundary conditions

Since each boundary condition has a different wavenumber dependence, the lined/lined configuration should be interpreted as a test of their predictive capability. Fig. 11 compares the axial wavenumbers $k(\omega)$ of the dominant duct modes predicted in the lined test section at $M = 0.3$, using the Ingard–Myers boundary condition. The difference between the axial wavenumbers when only one wall is lined or when both the top and bottom walls are lined is clear, and is especially dramatic for the upstream propagating mode. Similar results have been observed for $M = 0.2$, and therefore this demonstrates that the lined/rigid and lined/lined test cases really are significantly different, despite using the same impedance linings, frequencies, flow speeds, and other parameters.

We first test the Ingard–Myers boundary condition by comparing the experimental and predicted plane-wave scattering coefficients using the educed impedance from the lined/rigid configuration, as shown in

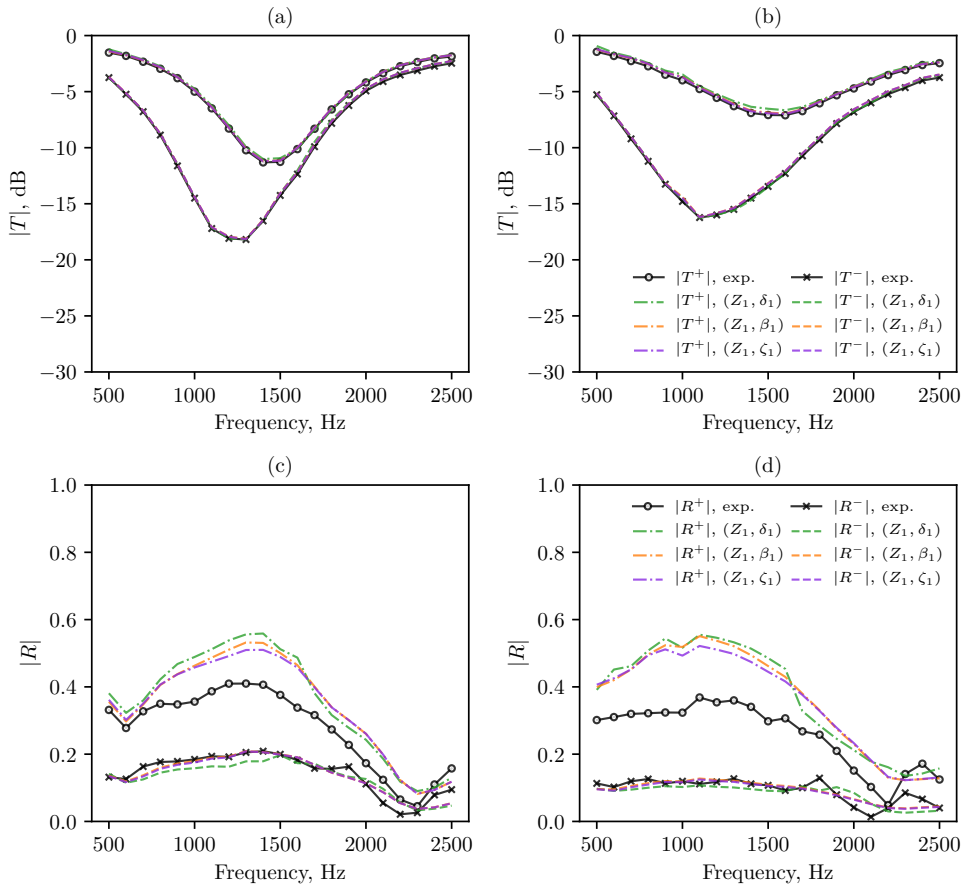

Figure 10: Experimental scattering coefficients for the lined/rigid configuration, and the predicted scattering coefficients using the educed two-parameters models from the same configuration. (a,c) $M = 0.2$; (b,d) $M = 0.3$.

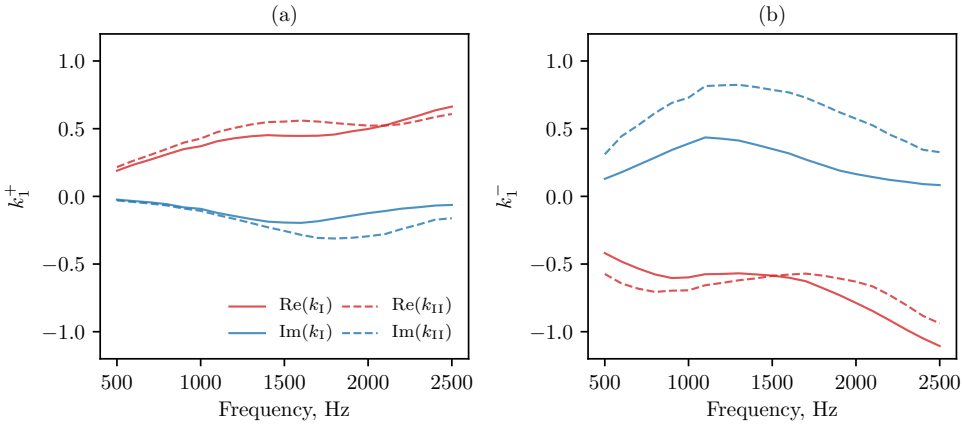

Figure 11: Educed axial wavenumbers of the most dominant downstream (+) and upstream (−) duct modes in the lined test section with a single lined wall (k_I), as a function of the frequency. Also shown are the predicted axial wavenumbers with two lined walls (k_II). (a) k_1^+, $M = 0.3$; (b) k_1^-, $M = 0.3$.

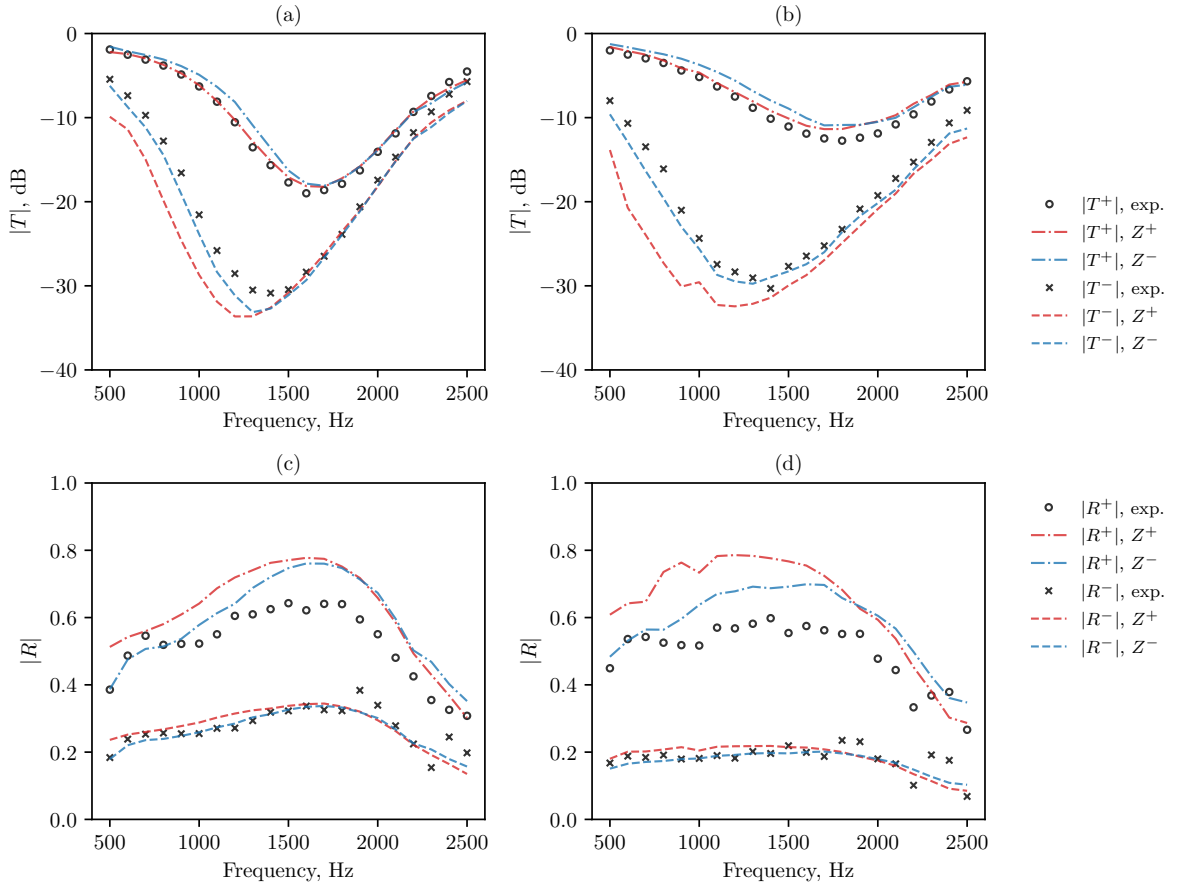

Figure 12: Experimental scattering coefficients for the lined/lined configuration, and the predicted scattering coefficients using the educed impedances from the lined/rigid configuration and considering Ingard-Myers boundary condition. (a,c) $M = 0.2$; (b,d) $M = 0.3$.

Fig. 12. Although we observe the same deficiency from the lined/rigid condition (where each educed impedance produces different scattering coefficients), the agreement between experiments and predictions is remarkable, as long as we use Z^+ to predict T^+, or Z^- to predict T^-. In other words, if there is a dominant propagation direction in an acoustic system, for instance the inlet of a turbofan engine, it may be sufficient to educe the liner impedance using the corresponding configuration in a test rig. In a more complicated acoustic environment where both upstream and downstream propagating waves are present, a more complicated boundary condition, such as the two-parameters models, may be necessary. Another striking feature of Fig. 12 is that both educed impedances lead to essentially the same R^-, which agrees well with the experiments, whereas the R^+ is once again poorly captured.

We now consider the predictions of the two-parameters impedance boundary conditions. As shown in Fig. 13, these models lead to very similar results, especially the β-factor (Z, β) and the momentum transfer impedance (Z, ζ). The biggest disparity is observed for the inviscid sheared boundary condition (Z, δ), as indicated by the reflections coefficients, although the disparity is still small. Surprisingly, none of the models are able to predict the maximum T^- at $M = 0.2$ and T^+ at $M = 0.3$. In order to highlight the difference between experimental and predicted transmission coefficients, Fig. 14 presents $\Delta|T^+|$ and $\Delta|T^-|$. It is interesting to note that the predictions with Ingard–Myers boundary condition are not distant from the other models, except for T^+ using Z^-, and for T^- using Z^+. Moreover, most of the discrepancy using Ingard–Myers is observed at frequencies below the liner resonance, which is in line with the theoretical

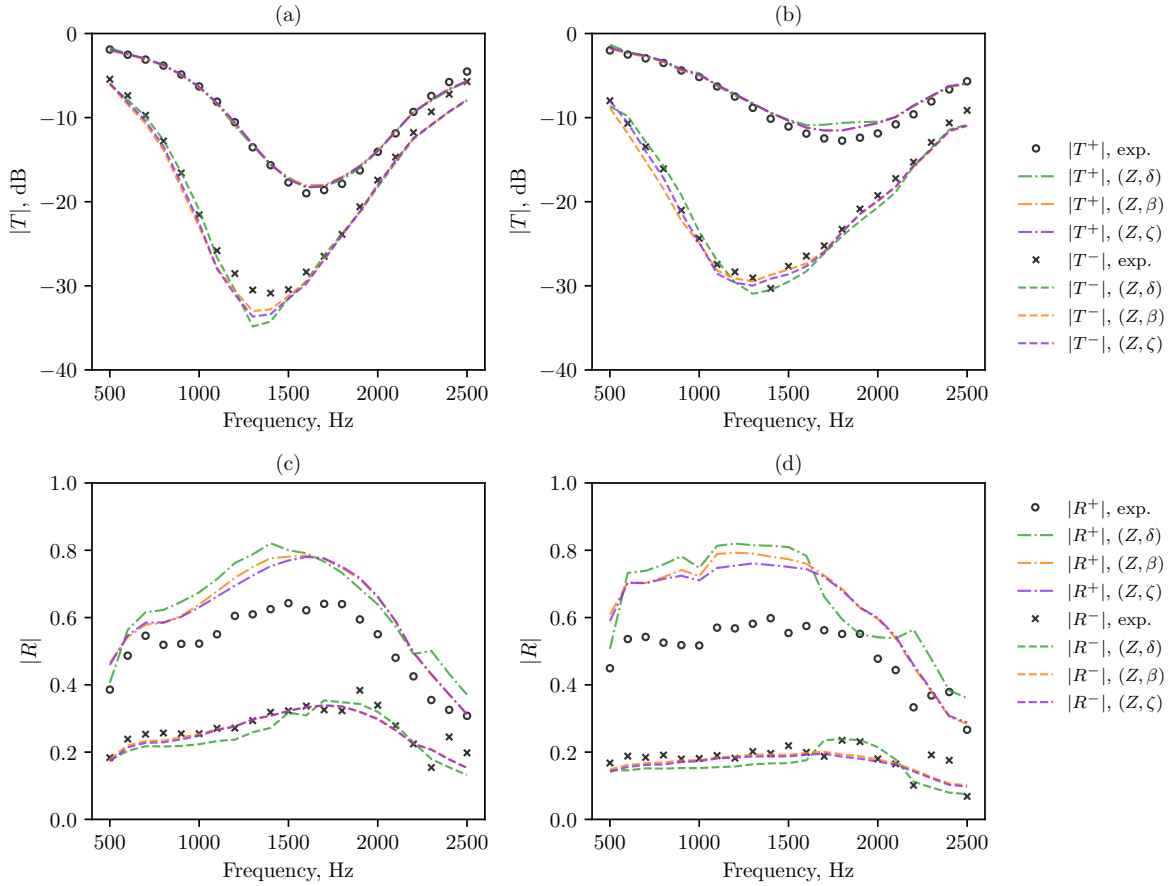

Figure 13: Experimental scattering coefficients for the lined/lined configuration, and the predicted scattering coefficients using the educed two-parameters models from the lined/rigid configuration. (a,c) $M = 0.2$; (b,d) $M = 0.3$.

prediction of β that continuity of acoustic velocity should be enforced instead of displacement in this regime.

6. Conclusions

In this work, several recently proposed impedance-like boundary conditions are tested, and compared with the traditional Ingard–Myers boundary condition. We consider the plane-wave scattering matrix as a quantitative parameter to test the impedance boundary conditions against experimental results.

The impedance eduction of nominally identical test samples assuming the Ingard–Myers boundary condition in a lined/rigid configuration was seen to lead to the well-reported discrepancies between upstream and downstream educed impedances, and the corresponding discrepancies between predicted upstream and downstream transmission coefficients $|T^+|$ and $|T^-|$ (Fig. 5). Boundary conditions based on inviscid sheared and viscous boundary layers, as well as acoustic shear stress at the lined wall, include an additional degree-of-freedom (either real or complex-valued), which can be tuned to collapse the upstream and downstream impedances. In this study, tuning these parameters has been found to lead to unphysical or unrealistic values (such as negative boundary layer thicknesses), raising questions regarding the correctness of such models. Indeed, since some of the models assume low Mach numbers and Helmholtz numbers, their theoretical validity may be limited, especially when applied to cases common in turbofan aeroengines. Nevertheless, these models were able to correctly predict both the upstream and downstream transmission coefficients $|T^+|$ and

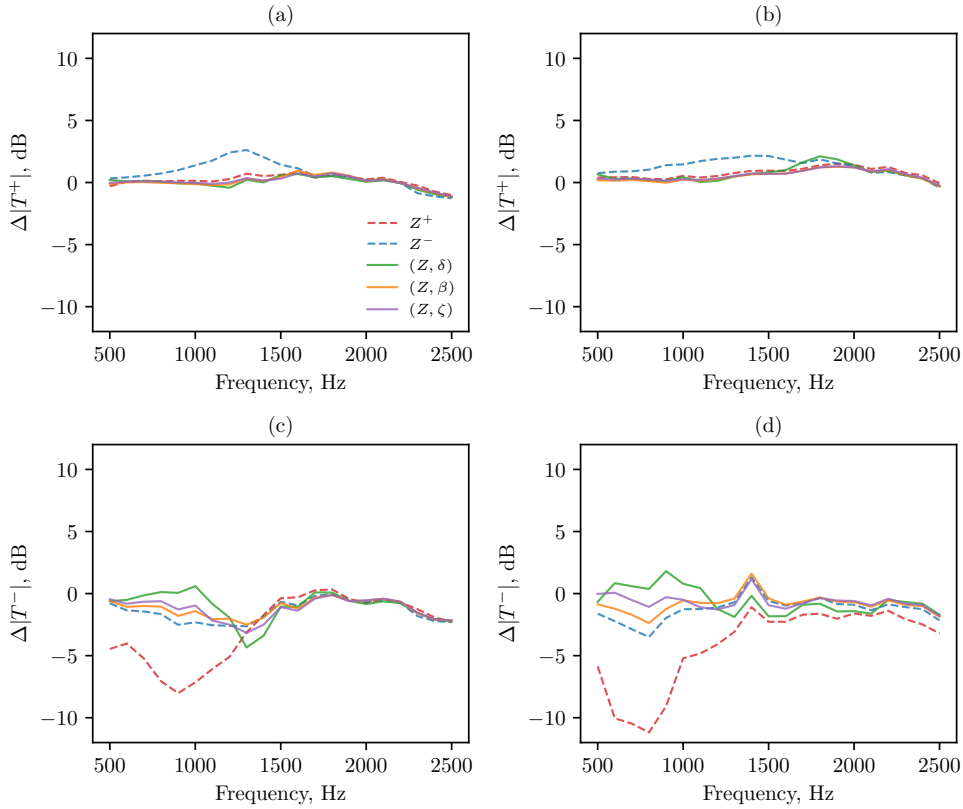

Figure 14: Difference between experimental and predicted transmission coefficients in the lined/lined configuration. (a,c) $M = 0.2$, (b,d) $M = 0.3$.

$|T^-|$ (as seen in Fig. 10). Since both upstream and downstream results are needed to educe the free parameters in these models, this correct prediction does not imply the correctness of the models. A correct model should also be accurate in different acoustic environments, such as an impedance educed in a lined/hard configuration being valid in a lined/lined configuration (with different wavenumbers but otherwise identical flow and acoustic parameters). Therefore, here the predictive capabilities of these models were tested by comparing the predicted and experimental scattering matrices obtained in a lined/lined configuration using parameters inferred from a lined/hard configuration. All of the models showed significantly worse agreement with the experiments in this case (compare Fig. 10 with Fig. 13), with both $|T^-|$ and $|T^+|$ showing inaccuracies of at least 3 dB in different cases (Figs. 13a and 13b) in the most important frequency regions where the liners have the highest attenuation. Furthermore, using Z^+ to predict T^+ leads to very similar errors in the transmission coefficient when compared to the two-parameter models, and similarly for Z^- and T^-. The closeness of the models make it difficult to say whether any of them is the most correct boundary condition. In fact, these results may suggest that the models are actually fitting some other physical effect. Therefore, the investigation of physically accurate boundary conditions for acoustic liners in the presence of flow remains an open topic.

During this study, it is observed that none of the boundary conditions are able to correctly predict the experimental reflection coefficient $|R^+|$ at the liner leading edge. This cannot be attributed to reflections from upstream of the test section, since the impedance eduction process used here did not assume anechoic terminations or other upstream or downstream boundary conditions, but rather reflections from outside the test section were included in the optimization to best fit the model to the observed experimental data. The inability to correctly predict the experimental reflection coefficients therefore highlights a more funda-

mental issue with the duct propagation model, perhaps related to boundary conditions or the uniform flow assumption.

Acknowledgments

The authors are grateful to Jose Alonso from UTC Aerospace Systems (now Collins Aerospace) for supplying the liner samples used in this study. AMNS, LAB and JAC gratefully acknowledge funding from CNPq (National Council for Scientific and Technological Development), FINEP (Funding Authority for Studies and Projects) and Embraer S.A. EJB gratefully acknowledges funding from a Royal Society University Research Fellowships (UF150695).

A preliminary version of some parts of this paper was presented as AIAA Paper 2019-2488 at the 25th AIAA/CEAS Aeroacoustics Conference in Delft, The Netherlands [1].

Appendix A. Elements of the mode matching matrices

The elements of matrices $\mathbf{P}_{\mathbf{i}}^{\pm}$ and $\mathbf{M}_{\mathbf{i}}^{\pm}$ in Eq. (17) are generically given by

$$\left(\mathbf{P}_{\mathbf{i}}^{\pm}\right)_{mn} = \left(1-M^2\right)\int_{-1}^{1}\overline{f}_m\psi_n^{(i)\pm}\,\mathrm{d}y \;+\; \frac{\mathrm{i}M^2}{\omega - Mk_n^{(i)\pm}}\left(\frac{\overline{f}_{b,m}\psi_{b,n}^{(i)\pm}}{Z_{\mathrm{eff},b,n}^{(i)\pm}} + \frac{\overline{f}_{t,m}\psi_{t,n}^{(i)\pm}}{Z_{\mathrm{eff},t,n}^{(i)\pm}}\right), \tag{A.1a}$$

$$\left(\mathbf{M}_{\mathbf{i}}^{\pm}\right)_{mn} = \frac{\left(1-M^2\right)k_n^{(i)\pm}}{\omega - Mk_n^{(i)\pm}}\int_{-1}^{1}\overline{f}_m\psi_n^{(i)\pm}\,\mathrm{d}y \;-\; \frac{\mathrm{i}M}{\omega - Mk_n^{(i)\pm}}\left(\frac{\overline{f}_{b,m}\psi_{b,n}^{(i)\pm}}{Z_{\mathrm{eff},b,n}^{(i)\pm}} + \frac{\overline{f}_{t,m}\psi_{t,n}^{(i)\pm}}{Z_{\mathrm{eff},t,n}^{(i)\pm}}\right), \tag{A.1b}$$

with $\psi_{b,n} \equiv \psi_n(-1)$ and $\psi_{t,n} \equiv \psi_n(1)$, and $Z_{\mathrm{eff},b}$ and $Z_{\mathrm{eff},t}$ denoting bottom and top wall effective impedances, respectively.

Although the mode shapes $\psi_n^{\pm}$ are given by the generalised eigenvalue problem, we consider the analytic solution,

$$\psi_n^{\pm}(y) = \mathrm{e}^{-\mathrm{i}\alpha_n^{\pm}y} + C_n^{\pm}\mathrm{e}^{\mathrm{i}\alpha_n^{\pm}y}, \tag{A.2}$$

with $C_n^{\pm}$ found by applying the desired boundary condition,

$$C_n^{\pm} = \begin{cases} \mathrm{e}^{-\mathrm{i}2\alpha_n^{\pm}} & \text{rigid at } y=1, \\ \mathrm{e}^{-\mathrm{i}2\alpha_n^{\pm}}\left(\dfrac{\omega - Mk_n^{\pm} - \alpha_n^{\pm}Z_{\mathrm{eff},n}^{\pm}}{\omega - Mk_n^{\pm} + \alpha_n^{\pm}Z_{\mathrm{eff},n}^{\pm}}\right) & \text{lined at } y=1. \end{cases} \tag{A.3}$$

In this way, closed-form solutions can be obtained for the integral terms, which are independent of the method used to compute the axial wavenumbers. In this work, rigid-walled acoustic modes are used as test functions since they form an orthogonal basis. The integral term is then, in the rigid-walled sections, given by

$$\int_{-1}^{1}\overline{f}_m\psi_n^{(1)\pm}\,\mathrm{d}y = \int_{-1}^{1}\overline{f}_m\psi_n^{(3)\pm}\,\mathrm{d}y = \begin{cases} 8, & \text{when } n=m=1, \\ 4, & \text{when } n=m\neq 1, \\ 0, & \text{when } n\neq m, \end{cases} \tag{A.4}$$

and, in the lined section,

$$\int_{-1}^{1}\overline{f}_m\psi_n^{(2)\pm}\,\mathrm{d}y = \frac{2\sin\left(\alpha_m^{(1)} - \alpha_n^{(2)\pm}\right)}{\alpha_m^{(1)} - \alpha_n^{(2)\pm}}\left(1 + \mathrm{e}^{\mathrm{i}2\alpha_m^{(1)}}C_n^{(2)\pm}\right) + \frac{2\sin\left(\alpha_m^{(1)} + \alpha_n^{(2)\pm}\right)}{\alpha_m^{(1)} + \alpha_n^{(2)\pm}}\left(\mathrm{e}^{\mathrm{i}2\alpha_m^{(1)}} + C_n^{(2)\pm}\right). \tag{A.5}$$

Finally, propagation and damping of each modal amplitude along the duct is considered by the propagation matrix,

$$\left(\mathbf{E}_{\mathbf{i}}^{\pm}(z)\right)_{nn} = \mathrm{e}^{-\mathrm{i}k_n^{(i)\pm}z}, \tag{A.6}$$

in which off-diagonal elements are zero.

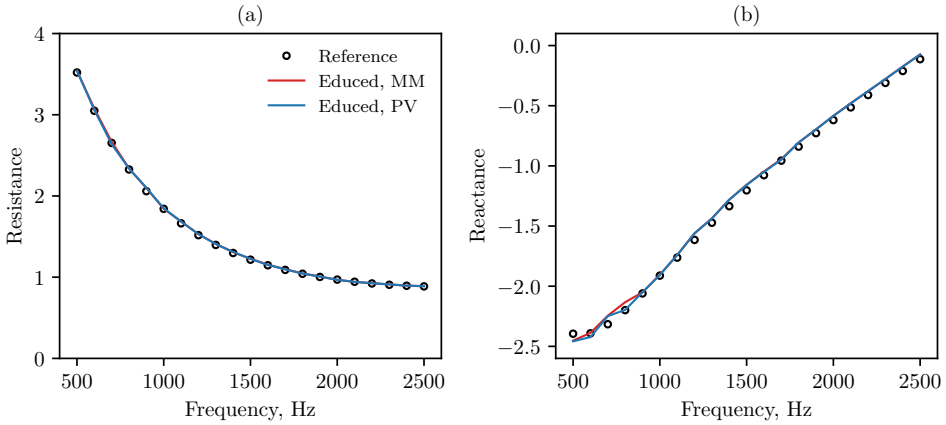

Figure B.15: Validation of the impedance eduction procedure using the mode-matching technique with $M = 0.25$, assuming matching of mass and momentum (MM) and pressure and velocity (PV). (a) Resistance; (b) reactance.

Appendix B. Validation of the impedance eduction procedure

In this section, the impedance eduction procedure is applied to an acoustic field obtained with a finite element method (FEM) given a known wall impedance Z using the commercial software COMSOL Multiphysics®. Since both mode-matching and FEM models are based on the same governing equations and boundary conditions, we expect the eduction procedure to return the exactly same impedance Z, which would also confirm the correct minimisation of the cost function. The three-dimensional duct geometry follows the same experimental setup, and terminations are anechoic. Probes are located at the exact same positions as the test rig microphones. A structured mesh with a minimum of 15 points per wavelength and quadratic shape functions is considered. The convected Helmholtz equation is solved in terms of velocity potential $\phi = \mathrm{i}p/(\omega - Mk)$ in a variational form. Following Jing et al. [31], measurement noise is added to the probes to better represent the experiments. As a reference case, we consider an uniform flow of velocity $M = 0.25$, an upstream acoustic source generating plane waves with frequencies between 500 and 2500 Hz, and a lined length of 0.2 m. Liner impedance is given by the Extended Helmholtz Resonator model [45] with coefficients obtained by Spillere et al. [36]. In addition to mass and momentum matching conditions, we also consider the commonly assumed continuity of pressure and velocity by neglecting the contour integral contribution.

The educed impedance is shown in Fig. B.15, where $\mathcal{N} = 10$ acoustic modes were used in the eduction. In general, the eduction procedure is able to correctly identify the liner impedance. Results near 500 Hz are sensitive to measurement noise due to a lower liner attenuation, and a perfect match occurs between educed and reference impedances when noise is removed. Similar conclusions are drawn when considering a downstream acoustic source. In terms of educed impedance, the choice of matching is of little importance, as long as the cost function is normalized by the measured pressure.

A second test of the impedance eduction procedure is to consider the scattering coefficients of the plane wave, $|T^{\pm}|$ and $|R^{\pm}|$. In this case, the coefficients obtained using the mode-matching technique with the educed impedance should match the reference FEM solution, which is shown in Fig. B.16a and B.16b. Finally, the model should be able to correctly predict a different condition, for instance in the presence of two lined walls with same impedance. Figs. B.16c and B.16d compare the scattering coefficients from the reference solution and the mode-matching technique with educed impedance from the single lined wall configuration. It should be noted that, when neglecting the contour contribution in Eqs. (A.1a) and (A.1b) (i.e. assuming continuity of pressure and velocity), the transmission coefficients remain well predicted, whereas the reflection coefficients are considerably inaccurate. This conclusion is in line with observations made by Gabard and Astley [37] and experimentally demonstrated by Yang et al. [38].

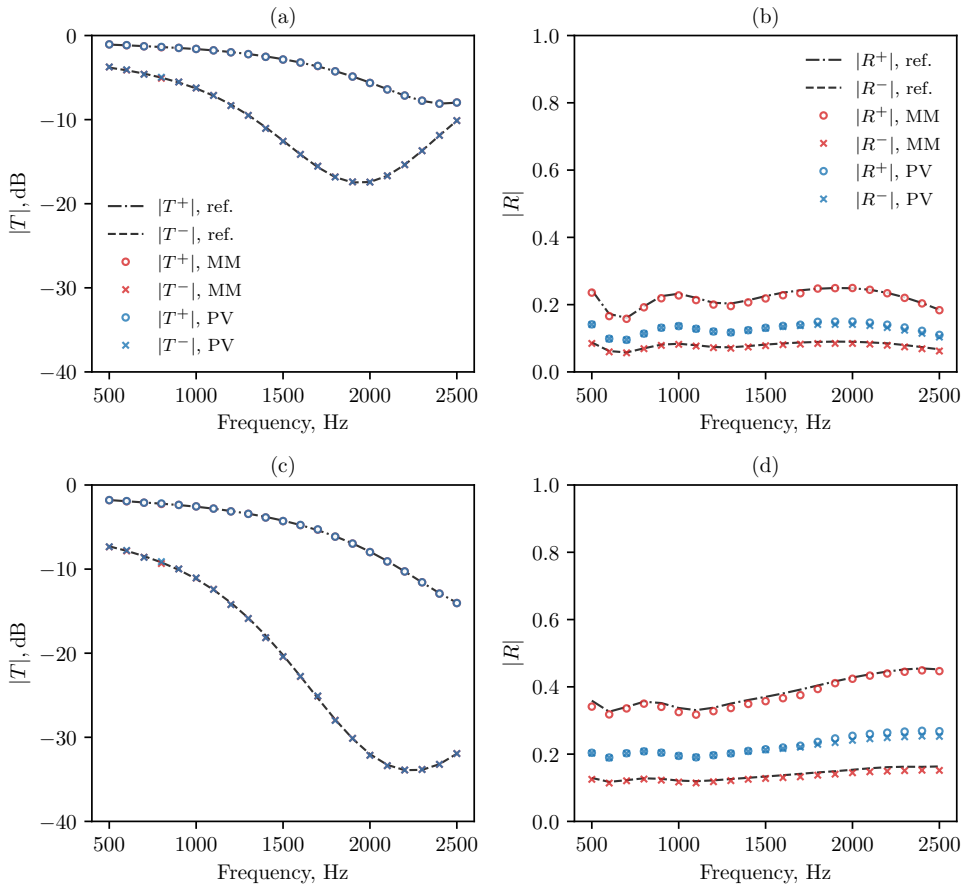

Figure B.16: Scattering matrix comparison between the reference solution and prediction using the mode-matching technique with $M = 0.25$, assuming matching of mass and momentum (MM) and pressure and velocity (PV). (a,b) single lined wall, (c,d) two lined walls.

Appendix C. Uncertainty estimates

In order to better understand whether the differences between upstream and downstream educed impedances could be explained by uncertainties in the test rig, a Monte Carlo method was applied to the impedance eduction procedure. It consists of including statistical properties to the measurement variables, such that the results are given by a mean educed impedance and a 95 % confidence interval. We assume a normal distribution on pressure, temperature, Mach number and microphone position, based on expected values of fabrication tolerances and experimental repeatability. A number of 1×10^3 Monte Carlo simulations was sufficient for convergence of statistical parameters.

Fig. C.17 shows the uncertainty intervals for the lined/rigid configuration using upstream and downstream sources without flow. The increased uncertainty at lower and higher frequencies is related to the low attenuation of the test sample at these frequencies. In this case, a wide range of impedances result in similar acoustic fields. Moreover, the liner supports acoustic surface waves at frequencies around 1.1 and 1.2 kHz, leading to ill-conditioned matrices in the mode matching method.

In the presence of flow, it is well reported in the literature that the educed impedances depends on the acoustic source location. The inclusion of confidence intervals, as shown in Fig. C.18, indicates that the difference between upstream and downstream educed impedances is not explained by measurement uncertainties up to frequencies around 2 kHz. These differences also persist at higher Mach numbers (omitted for brevity).

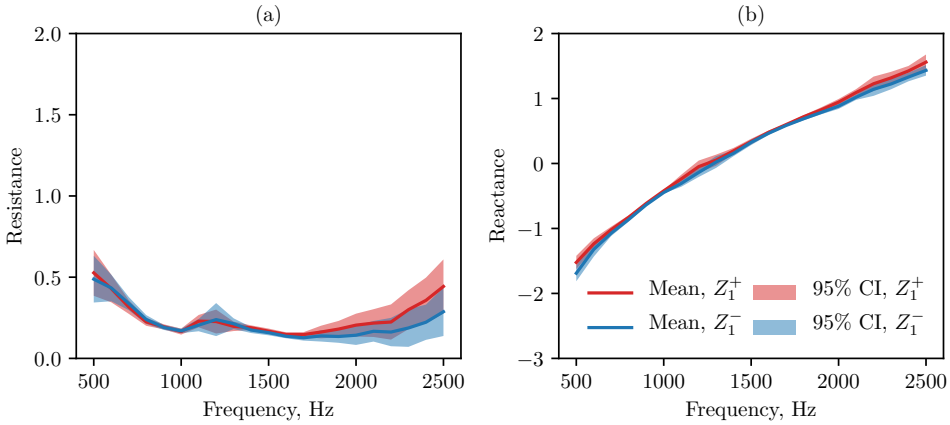

Figure C.17: Mean value and 95 % confidence interval of educed impedances in a lined/rigid (Z_1) configuration considering upstream (+) and downstream (−) sources without flow. (a) Educed resistance and (b) educed reactance.

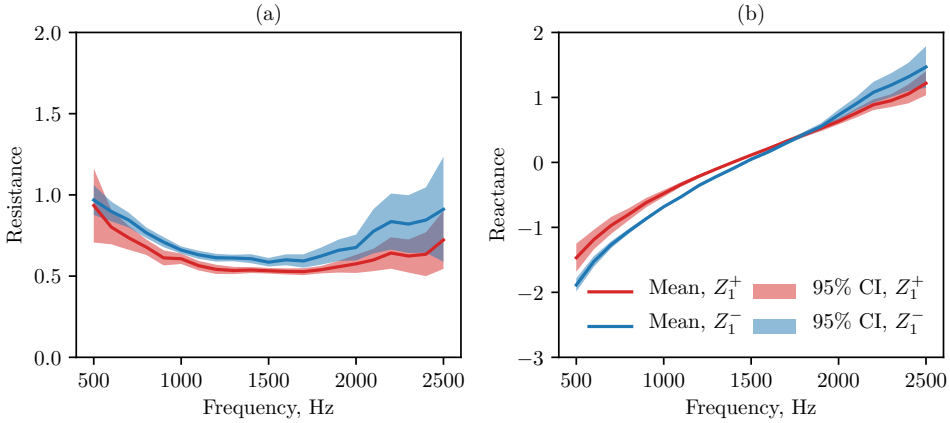

Figure C.18: Mean value and 95 % confidence interval of educed impedances in a lined/rigid (Z_1) configuration considering upstream (+) and downstream (−) sources with $M = 0.2$. (a) Educed resistance and (b) educed reactance.

Finally, small differences in the educed impedance have been observed between lined/rigid and rigid/lined configurations, specially in the presence of flow. Fig. C.19 shows the educed impedances with confidence intervals for both test samples with an upstream acoustic source. The difference between mean educed impedances is well within the limits of the confidence interval, which highlights the measurement repeatability. Similar results have been observed with a downstream acoustic source and at higher Mach numbers.

References

[1] A. M. N. Spillere, L. A. Bonomo, J. A. Cordioli, E. J. Brambley, Testing impedance eduction boundary conditions with four wavenumbers per frequency, AIAA paper 2019-2488 (2019). doi:10.2514/6.2019-2488.

[2] Y. Renou, Y. Aurégan, Failure of the Ingard–Myers boundary condition for a lined duct: An experimental investigation, J. Acoust. Soc. Am. 130 (2011) 52–60. doi:10.1121/1.3586789.

[3] H. Bodén, L. Zhou, J. A. Cordioli, A. A. Medeiros, A. M. N. Spillere, On the effect of flow direction on impedance eduction results, AIAA paper 2016-2727 (2016). doi:10.2514/6.2016-2727.

[4] C. Weng, A. Schulz, D. Ronneberger, L. Enghardt, F. Bake, Flow and viscous effects on impedance eduction, AIAA J. 56 (3) (2017) 1118–1132. doi:10.2514/1.J055838.

[5] U. Ingard, Influence of fluid motion past a plane boundary on sound reflection, absorption, and transmission, J. Acoust. Soc. Am. 31 (1959) 1035–1036. doi:10.1121/1.1907805.

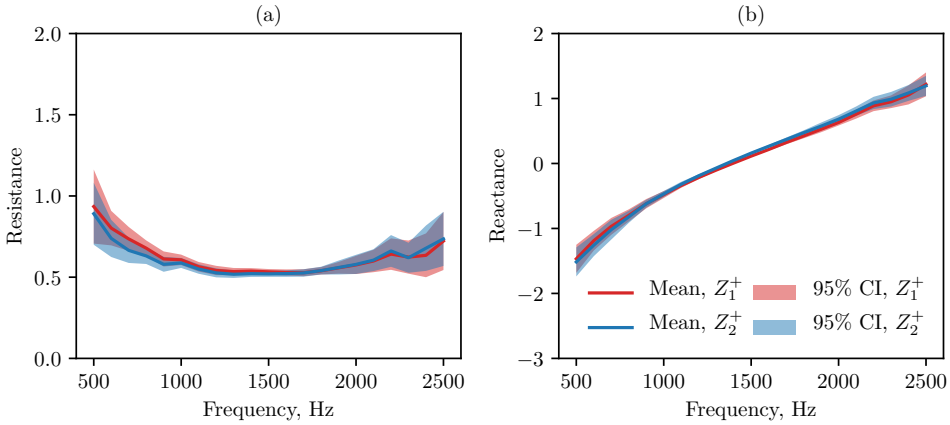

Figure C.19: Mean value and 95 % confidence interval of educed impedances in a lined/rigid (Z_1) and rigid/lined (Z_2) configurations considering upstream (+) source with $M = 0.2$. (a) Educed resistance and (b) educed reactance.

[6] M. K. Myers, On the acoustic boundary condition in the presence of flow, J. Sound Vib. 71 (1980) 429–434. doi:10.1016/0022-460X(80)90424-1.

[7] D. M. Nark, M. G. Jones, E. Piot, Assessment of axial wave number and mean flow uncertainty on acoustic liner impedance eduction, AIAA paper 2018-3444 (2018). doi:10.2514/6.2018-3444.

[8] R. Roncen, E. Piot, F. Méry, F. Simon, M. G. Jones, D. M. Nark, Wavenumber-based impedance eduction with a shear grazing flow, AIAA J. 58 (7) (2020) 3040–3050. doi:10.2514/1.J059100.

[9] J. Rebel, D. Ronneberger, The effect of shear stress on the propagation and scattering of sound in flow ducts, J. Sound Vib. 158 (3) (1992) 469 – 496. doi:10.1016/0022-460X(92)90420-3.

[10] Y. Aurégan, R. Starobinski, V. Pagneux, Influence of grazing flow and dissipation effects on the acoustic boundary conditions at a lined wall, J. Acoust. Soc. Am. 109 (2001) 59–64. doi:10.1121/1.1331678.

[11] W. Eversman, R. J. Beckemeyer, Transmission of sound in ducts with thin shear layers—convergence to the uniform flow case, J. Acoust. Soc. Am. 52 (1B) (1972) 216–220. doi:10.1121/1.1913082.

[12] J. Yu, M. Ruiz, H.-W. Kwan, Validation of Goodrich perforate liner impedance model using NASA Langley test data, AIAA paper 2008-2930 (2008). doi:10.2514/6.2008-2930.

[13] P. Murray, R. J. Astley, Development of a single degree of freedom perforate impedance model under grazing flow and high SPL, AIAA paper 2012-2294 (2012). doi:10.2514/6.2012-2294.

[14] E. J. Brambley, Fundamental problems with the model of uniform flow over acoustic linings, J. Sound Vib. 322 (2009) 1026–1037. doi:10.1016/j.jsv.2008.11.021.

[15] A. M. N. Spillere, J. A. Cordioli, H. Bodén, On the effect of boundary conditions on impedance eduction results, AIAA paper 2017-3185 (2017). doi:10.2514/6.2017-3185.

[16] E. J. Brambley, Acoustic implications of a thin viscous boundary layer over a compliant surface or permeable liner, J. Fluid Mech. 678 (2011) 348–378. doi:10.1017/jfm.2011.116.

[17] D. Khamis, E. J. Brambley, Viscous effects on the acoustics and stability of a shear layer over an impedance wall, J. Fluid Mech. 810 (2017) 489–534. doi:10.1017/jfm.2016.737.

[18] D. Khamis, E. J. Brambley, Acoustics in a two-deck viscothermal boundary layer over an impedance surface, AIAA J. 55 (10) (2017) 3328–3345. doi:10.2514/1.J055598.

[19] A. Schulz, C. Weng, F. Bake, L. Enghardt, D. Ronneberger, Modeling of liner impedance with grazing shear flow using a new momentum transfer boundary condition, AIAA paper 2017-3377 (2017). doi:10.2514/6.2017-3377.

[20] Y. Aurégan, On the use of a stress–impedance model to describe sound propagation in a lined duct with grazing flow, J. Acoust. Soc. Am. 143 (5) (2018) 2975–2979. doi:10.1121/1.5037585.

[21] A. A. Medeiros, J. A. Cordioli, Evaluation of three impedance eduction methods for acoustic liners under grazing flow, in: Proceedings of EuroNoise 2015, Maastricht, 2015, pp. 2297–2302.

[22] K. Shin, J. Hammond, Fundamentals of signal processing for sound and vibration engineers, Wiley, Chichester, UK, 2008.

[23] G. Krishnappa, Cross-spectral method of measuring acoustic intensity by correcting phase and gain mismatch errors by microphone calibration, J. Acoust. Soc. Am. 69 (1981) 307–310. doi:10.1121/1.385314.

[24] ISO Central Secretary, Measurement of fluid flow in closed conduits — Velocity area method using Pitot static tubes, Standard ISO 3966:2008, International Organization for Standardization, Geneva, Switzerland (2008).
URL https://www.iso.org/standard/50626.html

[25] H. Schlichting, Boundary-layer theory, 6th Edition, McGraw-Hill, New York, 1968.

[26] G. Gabard, A comparison of impedance boundary conditions for flow acoustics, J. Sound Vib. 332 (4) (2013) 714 – 724. doi:10.1016/j.jsv.2012.10.014.

[27] A. Nayfeh, J. Kaiser, B. Shaker, Effect of mean-velocity profile shapes on sound transmission through two-dimensional

ducts, J. Sound Vib. 34 (3) (1974) 413 – 423. doi:10.1016/S0022-460X(74)80320-2.
[28] T. Elnady, H. Bodén, B. Elhadidi, Validation of an inverse semi-analytical technique to educe liner impedance, AIAA J. 47 (2) (2009) 2836–2844. doi:10.2514/1.41647.
[29] Y. Aurégan, M. Leroux, V. Pagneux, Measurement of liner impedance with flow by an inverse method, AIAA paper 2004-2838 (2004). doi:10.2514/6.2004-2838.
[30] M. G. Jones, W. R. Watson, Effects of liner length and attenuation on nasa langley impedance eduction, AIAA paper 2016-2782 (2016). doi:10.2514/6.2016-2782.
[31] X. Jing, S. Peng, X. Sun, A straightforward method for wall impedance eduction in a flow duct, J. Acoust. Soc. Am. 124 (1) (2008) 227–234. doi:10.1121/1.2932256.
[32] S. W. Rienstra, A classification of duct modes based on surface waves, Wave Motion 37 (2) (2003) 119 – 135. doi:10.1016/S0165-2125(02)00052-5.
[33] J. Boyd, Chebyshev and Fourier Spectral Methods: Second Revised Edition, Dover Books on Mathematics, Dover Publications, 2001.
[34] W. R. Watson, M. G. Jones, T. L. Parrott, Investigation of an anomaly observed in impedance eduction techniques, AIAA paper 2008-3013 (2008). doi:10.2514/6.2008-3013.
[35] Y. Buot de l'Épine, J.-D. Chazot, J.-M. Ville, Bayesian identification of acoustic impedance in treated ducts, J. Acoust. Soc. Am. 138 (1) (2015) EL114–EL119. doi:10.1121/1.4923013.
[36] A. M. N. Spillere, A. A. Medeiros, J. A. Cordioli, An improved impedance eduction technique based on impedance models and the mode matching method, Applied Acoustics 129 (2018) 322 – 334. doi:10.1016/j.apacoust.2017.08.014.
[37] G. Gabard, R. Astley, A computational mode-matching approach for sound propagation in three-dimensional ducts with flow, J. Sound Vib. 315 (4) (2008) 1103 – 1124. doi:10.1016/j.jsv.2008.02.015.
[38] C. Yang, Y. Fang, C. Zhao, X. Zhang, On modeling the sound propagation through a lined duct with a modified ingard-myers boundary condition, J. Sound Vib. 424 (2018) 173 – 191. doi:10.1016/j.jsv.2018.03.022.
[39] A. Cummings, High frequency ray acoustics models for duct silencers, J. Sound Vib. 221 (4) (1999) 681 – 708. doi:10.1006/jsvi.1999.2030.
[40] M. Åbom, Measurement of the scattering-matrix of acoustical two-ports, Mechanical Systems and Signal Processing 5 (2) (1991) 89 – 104. doi:10.1016/0888-3270(91)90017-Y.
[41] E. Dokumaci, Sound transmission in narrow pipes with superimposed uniform mean flow and acoustic modelling of automobile catalytic converters, J. Sound Vib. 182 (5) (1995) 799 – 808. doi:10.1006/jsvi.1995.0233.
[42] K. Levenberg, A method for the solution of certain non-linear problems in least squares, Quarterly of Applied Mathematics 2 (2) (1944) 164–168. doi:10.1090/qam/10666.
[43] D. W. Marquardt, An algorithm for least-squares estimation of nonlinear parameters, Journal of the Society for Industrial and Applied Mathematics 11 (2) (1963) 431–441. doi:10.1137/0111030.
[44] O. Léon, F. Méry, E. Piot, C. Conte, Near-wall aerodynamic response of an acoustic liner to harmonic excitation with grazing flow, Experiments in Fluids 60 (144). doi:10.1007/s00348-019-2791-5.
[45] S. W. Rienstra, Impedance models in time domain, including the extended Helmholtz resonator model, AIAA paper 2006-2686 (2006). doi:10.2514/6.2006-2686.